Bioresource Technology 284 (2019) 466–473

Contents lists available at ScienceDirect

Bioresource Technology

journal homepage: www.elsevier.com/locate/biortech

Kinetics, thermodynamics, and physical characterization of corn stover (*Zea mays*) for solar biomass pyrolysis potential analysis

Asif Hasan Rony[a], Lingli Kong[a], Wenyang Lu[a], Morteza Dejam[b], Hertanto Adidharma[a,b], Khaled A.M. Gasem[a,b], Yuan Zheng[d], Urszula Norton[c], Maohong Fan[a,b,e,f,*]

[a] Department of Chemical Engineering, University of Wyoming, Laramie, WY 82071, USA
[b] Department of Petroleum Engineering, University of Wyoming, Laramie, WY 82071, USA
[c] Department of Plant Sciences, University of Wyoming, Laramie, WY 82071, USA
[d] Department of Mechanical Engineering, University of Wyoming, Laramie, WY 82071, USA
[e] School of Energy Resources, University of Wyoming, Laramie, WY 82071, USA
[f] School of Civil and Environmental Engineering, Georgia Institute of Technology, Atlanta, GA 30332, USA

GRAPHICAL ABSTRACT

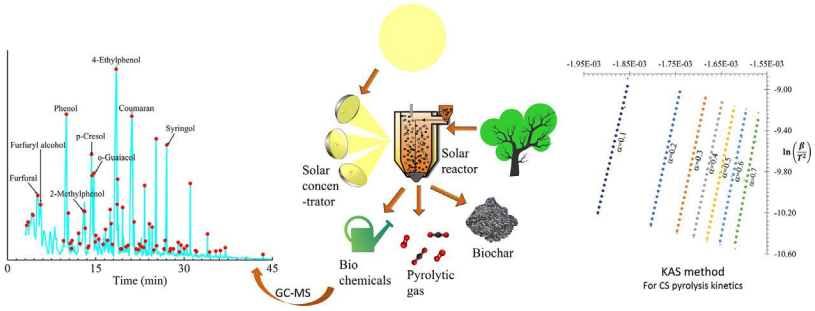

ARTICLE INFO

Keywords:
Corn stover
Solar pyrolysis
Kinetics
Thermodynamics

ABSTRACT

Solar pyrolysis of agricultural waste has huge potential for sustainable production of fuel and chemical feedstock. In this paper, the kinetics, thermodynamics, and physical characterization of corn stover (CS) collected from Wyoming, USA was conducted with respect to solar pyrolysis. The kinetics and thermodynamics of the CS pyrolysis was analyzed in detail using the methods described by KAS (Kissinger-Akahira-Sunose) and FWO (Flynn-Wall-Ozawa), from which the activation energy, Gibbs energy, Arrhenius pre-exponential factor, enthalpy, and entropy were derived.14 other kinetics models based on reaction order, diffusion, nucleation, geometric contraction, power models were also examined, and models based on diffusion was found to be best suited. The CS was used for solar pyrolysis of biomass and the products were analyzed by mass spectroscopy, ICP-MS, GPC, micro-GC, and Elemental analyzer. The results show that CS is suitable for solar pyrolysis to produce chemicals and other fuels.

1. Introduction

The concept of global warming has raised worldwide concerns regarding energy consumptions and utilization efficiency in recent years. Although energy efficiency is improving continuously, the demand for energy is increasing more rapidly. Moreover, the lion's share

* Corresponding author at: Department of Petroleum Engineering, EN4015, Dept. 3295, 1000 E University Ave., Laramie, WY 82071, USA.
E-mail address: mfan@uwyo.edu (M. Fan).

https://doi.org/10.1016/j.biortech.2019.03.049
Received 20 January 2019; Received in revised form 8 March 2019; Accepted 9 March 2019
Available online 15 March 2019
0960-8524/

of global energy consumption is still based on fossil fuel (Angel Gurría, 2012). The emissions from fossil fuel possess a serious threat to the world climate. Despite a huge amount of effort on a global scale, a way to regulate humanity out of the climate problem is yet to be found. Luckily, renewable energy is paving its way for a sustainable earth. Renewable technologies such as bio-fuel (Bridgwater, 2012), solar (Chintala et al., 2017; Yadav and Banerjee, 2016), wind, hydro are gradually replacing fossil fuels (Foley and Olabi, 2017).

Bio-fuels are derived from non-fossilized bio-degradable organic matter from plant or animal origins (UNFCCC, 2015). The sources can be classified in two categories such as virgin (energy crops) and bio-waste (Agricultural waste or municipal waste) (Fantini, 2017). Biomass is often defined as a lignocellulosic material as it contains lignin (10–25%), cellulose (32–50%), hemicellulose (19–30%), and other organic extractives (Anwar et al., 2014), each of which has distinct physical and thermal properties (Chen et al., 2014; Wang et al., 2017; Zeng et al., 2017). Cellulose consists of linear chain polysaccharide, hemicellulose is made of branched structured amorphous sugar units, while lignin has cross-linked complex polymer structure containing phenolic groups.

As biomass material is often less energy dense, combustion for extracting energy is not ideal (Weldekidan et al., 2018). Pyrolysis and gasification processes through thermochemical conversion can improve the energy density significantly (Bridgwater, 2003). In this paper, our focus will remain on biomass pyrolysis only. Pyrolysis is a thermochemical process where an organic material is subject to intense heat under anaerobic condition. The product stream consists of char, gas, water, bio-oil, and tar. The most common modes of pyrolysis include torrification, fast pyrolysis, and flash pyrolysis. To run a pyrolysis process, significant heat input is necessary. Typically, the heating source is electricity from non-renewable sources. But recent advances in solar technology makes it a potential candidate for heating viable solar thermochemical processes (Sánchez et al., 2018; Zeng et al., 2017). Zeng et al. evaluated the solar pyrolysis of several feedstocks including biomass and coal. According to the study, at higher temperature solar furnaces can be used to produce gaseous products however a lower temperature can produce more liquid products (Chintala, 2018). Yadav and Banerjee reviewed the solar pyrolysis focusing experimental demonstrations, technologies related to reactor development, thermodynamics, and life cycle analysis. Specifically, they have addressed multistep thermodynamic cycles, performances of various metal oxides during thermochemical cycles, efficiency of various solar powered processes, and the production cost comparison between solar and non-solar thermochemical applications. Meier and Steinfeld (Meier and Steinfeld, 2010) studied the solar thermochemical conversion for production of valuable fuels such as hydrogen and CO at a higher temperature. The process can be commercially competitive if credits for CO2 mitigation is available. Sánchez et al. evaluated solar pyrolysis using linear Frensnel reflector (LFR) system. They have estimated the ideal temperature, total residence time, reactor size, solar concentrator aperture size for maximization of char production.

Among plant-based biomass sources, water born plants, municipal waste, and agricultural waste are the potential candidate to produce bio-oil using thermochemical conversion as those do not directly compete with human food. In the USA, CS is the most available (109 million tons) plant-based biomass (Perlack and Stokes, 2011). Most of these are used as landfill, animal feeds, and animal bedding. According to literature, about 33% of the CS can be removed without serious effect on the soil quality and GHG (Green House Gas) emission target (Kim et al., 2018). Many places, especially in the south-western region of the USA, corn is popular as a crop (Kim and Dale, 2016) and has a higher amount of solar light availability. As corn is a popular bio-ethanol producing source, there are a number of literatures covering the importance of corn stover (CS) as a potential thermochemical conversion feed (Biney et al., 2015; Cai et al., 2018; Mishra and Mohanty, 2018). Rafiq et al. (2016) described the physical and chemical properties of CS in terms of carbon capture and biochar production. Tae Hyun Kim et al. (Kim et al., 2003) studied the pretreatment of corn stover with ammonia solution in a flow-through column reactor in an attempt to delignify biomass to enhance enzymatic digestibility. Kim and Holtzapple (Kim and Holtzapple, 2005) described lime pretreatment and enzymatic hydrolysis of corn stover to improve mono-sugar productions. Tao et al. (Tao et al., 2014) performed a techno-economic analysis for production of n-buanol from corn stover. Sheehan et al. (Sheehan et al., 2003) studied the ethanol production from corn stover in light of energy and environmental aspect. Pordesimo et al. (Pordesimo et al., 2005) found that composition corn stover and energy value is a function of crop maturity. Specifically, soluble solids, lignin content, and xylan content was most notable when the grain physiological maturity was varied. Templeton et al (Templeton et al., 2009) assessed the variability of corn stover composition using near infrared spectroscopy. It was reported that, there is wide variety in corn stover composition collected from different region from the USA when measured for glucan, xylan, soluble components, and lignin.

Mishra and Mohanty (Mishra and Mohanty, 2018) described the CS using FWO (Flynn-Wall-Ozawa), KAS (Kissinger-Akahira-Sunose) and (Distributed Activation Energy Model) DAEM model. Biney et al. (2015) described the kinetics of CS using multi-stage model. Both of these studies calculated the activation energy, Arrhenius pre-exponential factor for CS. However, none of these works focused on the solar bio-fuel potential of CS. Thus, this research was developed to make progress in filling the gap.

2. Materials and methods

2.1. Material characterization

2.1.1. Ultimate and proximate analysis

CS used for this research was collected from a research field of the University of Wyoming. The CS was cleaned, chopped, crushed, sieved, and dried. For all the experiments reported in this paper, size of the samples was between mesh 35-140. Section 3.1 shows the mean value of the proximate and ultimate analysis conducted several times. ASTM D3172-13 standard was used for proximate analysis of CS powder (ASTM D3172-13 Standard Practice for Proximate Analysis of Coal and Coke, 2013). A TGA-SDT Q600 was used for the proximate analysis of 2.0 mg samples at different heating rates. The definitions of moisture content, volatile, ash content, and fixed carbon are shown as follows

$$\text{Moisture Content, } MC(\%) = \frac{W - B}{W} * 100\% \quad (1)$$

$$\text{Volatile, } V(\%) = \frac{B - C}{W} * 100\% \quad (2)$$

$$\text{Ash content, } A(\%) = \frac{F}{W} * 100\% \quad (3)$$

$$\text{Fixed carbon, } FC(\%) = 100\% - \{MC(\%) + V(\%) + A(\%)\} \quad (4)$$

where W is the mass of original test specimen, B is the test specimen after drying in moisture test, C is the mass of test specimen after heating in volatile matter test, F is the mass of ash residue. Each test was conducted three times and the average value of the data from the three tests was reported. The ultimate analysis was done by a 'Vario MACRO Cube CHNOS Elemental Analyzer'. About 50 mg of samples were completely burned using oxygen.

2.1.2. Inductively coupled plasma mass spectrometry (ICP-MS)

For the ash analysis of CS, first the CS samples were burnt in an incinerator under atmospheric condition. The ash then added to a mixture of HF (49%), HCl (38%), and HNO_3 (69%). The ash liquid mixture was then heated in a silicone oil bath up to 80 °C to ensure the dissolution of all solids. After that, the mixture was cooled down and

Table 1
Fitting performance of various kinetics model for CS pyrolysis.

Sl.	Kinetics models	Differential form f (α)	Integral form g (α)	R^2 range ($0 \le \alpha < 0.75$)	R^2 range ($0.75 \le \alpha < 1.0$)
Diffusion models					
1	1-D diffusion	$\frac{1}{2}(1-\alpha)-1$	α^2	0.9298–0.9514	0.9502–0.9694
2	2-D diffusion	$-\ln(1-\alpha)$	$\{(1-\alpha)\ln(1-\alpha)\}+\alpha$	0.9351–0.9554	0.8862–0.9475
3	3-D diffusion-Jander	$\frac{3}{2}(1-\alpha)^{2/3}\{1-(1-\alpha)^{2/3}\}^{-1}$	$\{1-(1-\alpha)^{1/3}\}^2$	0.9401–0.9589	0.0003–0.5644
Geometrical contraction models					
4	Contracting area	$2(1-\alpha)^{1/2}$	$1-(1-\alpha)^{1/2}$	0.9280–0.9496	0.9661–0.9853
5	Contracting volume	$3(1-\alpha)^{2/3}$	$1-(1-\alpha)^{1/3}$	0.9309–0.9517	0.9463–0.9743
Reaction-order models					
6	Zero order	1	α	0.9186–0.9423	0.9815–0.9865
7	1st order	$(1-\alpha)$	$-\ln(1-\alpha)$	0.9361–0.9554	0.0059–0.3548
8	2nd order	$(1-\alpha)^2$	$\frac{1}{1-\alpha}-1$	0.9468–0.9617	0.5601–0.6761
Power models					
9	P2	$2\alpha^{1/2}$	$\alpha^{1/2}$	0.8880–0.9173	0.9894–0.9908
10	P3	$3\alpha^{2/3}$	$\alpha^{1/3}$	0.8403–0.8773	0.9913–0.9920
11	P4	$4\alpha^{3/4}$	$\alpha^{1/4}$	0.7626–0.8077	0.9921–0.9926
Nucleation models					
12	Avrami-Erofeyev (A2)	$2(1-\alpha)\{-\ln(1-\alpha)\}^{1/2}$	$-\{\ln(1-\alpha)\}^{1/2}$	0.9135–0.9380	0.9549–0.9718
13	Avrami-Erofeyev (A3)	$3(1-\alpha)\{-\ln(1-\alpha)\}^{2/3}$	$-\{\ln(1-\alpha)\}^{1/3}$	0.8787–0.9099	0.9861–0.9922
14	Avrami-Erofeyev (A4)	$4(1-\alpha)\{-\ln(1-\alpha)\}^{3/4}$	$-\{\ln(1-\alpha)\}^{1/4}$	0.8225–0.8620	0.9917–0.9954

boric acid was added to remove additional F^-. The mixture was diluted using deionized (DI) water. A Perkin Elmer® Nexion 300 ICP-MS instrument was used for the ash analysis. The instrument was operated under standard mode and all analyses were completed using external standards and Rhenium (Re) was used as the internal standard.

2.1.3. Thermogravimetric analysis (TGA)

The TGA analysis was conducted using a TGA-SDT Q600. Ultra-pure nitrogen gas at a flow rate of 100 ml/min was used to provide the inert condition for the CS. The sample was dried for 24 h before being placed inside the thermogravimetric (TG) chamber. The temperature was increased at a constant heating rate from room temperature to 900 °C. After the sample was kept at a constant temperature (900 °C) for several minutes (5 min) before being heated to 1000 °C. At constant temperature, air is introduced inside the chamber to burn off any volatile materials from the system. The operation was repeated for several heating rates (10 k/min, 20 k/min, 30 k/min, and 40 k/min).

2.2. Kinetics of CS pyrolysis

The chemical reaction rate dα/dT is generally expressed as

$$\frac{d\alpha}{dt} = k(T)f(\alpha) \tag{5}$$

where f(α) is function related to conversion, T is the temperature (K), and α represents the degree of conversion that is described as

$$\alpha = \frac{m_i - m_t}{m_i - m_f} \tag{6}$$

where m_i, m_t, and m_f are the initial mass of the sample, the actual mass of the sample at time t, and the final mass of the sample in the reaction. Arrhenius equation express $k(T)$ as

$$k = Aexp^{\left(-\frac{E_a}{RT}\right)} \tag{7}$$

where A (s^{-1}) is the Arrhenius pre-exponential factor, E_a (J/mol) is the activation energy of pyrolysis reaction, and R ($J\,mol^{-1}\,K^{-1}$) is the universal gas constant. The combination of Eqs. (5) and (7) gives

$$\frac{d\alpha}{dt} = Aexp^{\left(-\frac{E_\alpha}{RT}\right)}f(\alpha). \tag{8}$$

Integrating the heating rate β (K/min) defined as

$$\beta = \frac{dT}{dt} \tag{9}$$

with Eq. (9) leads to

$$\frac{d\alpha}{dT} = \frac{A}{\beta}exp^{\left(-\frac{E_a}{RT}\right)}f(\alpha) \tag{10}$$

The integrated form of Eq. (11) is

$$G(\alpha) = \int_0^\alpha \frac{d}{f(\alpha)} = \frac{A}{\beta}\int_{T_0}^{T} exp\left(-\frac{E_a}{RT}\right)dT \tag{11}$$

$$T = T_0 + \beta\ t \tag{12}$$

where T_0(K) and f(α) are initial temperature and conversion function, respectively.

2.2.1. Kinetics models

Coats-Redfern (CR) method (COATS and REDFERN, 1964) can be approximated as

$$\ln\left(\frac{g(\alpha)}{T^2}\right) = \ln\left(\frac{k_0R}{\beta E_a}\right) - \frac{E_a}{RT} \tag{13}$$

g(α) can be varied according to the kinetics model and from $\ln\left(\frac{g(\alpha)}{T^2}\right)$ vs $1/T$ *plot,* activation energy *(E_a)* and rate constant *(k_0)* can be calculated. A number of kinetics models were selected as shown in Table 1. The models were fitted using MATLAB® and R^2 value was calculated.

2.2.2. Model free methods

It is well-known that the iso-conversional method can easily give an estimation of E even without knowing the associated reaction mechanism. Thus, two iso-conversional methods, FWO and KAS methods were used for activation energy calculation due to the relatively high reliability themselves. The FWO method can be described as:

$$ln\beta = \ln\left(\frac{0.0048AE_\alpha}{Rg(\alpha)}\right) - 1.0516\frac{E_\alpha}{RT_\alpha} \tag{14}$$

where for a chosen value of α, the values of lnβ and $1/T_\alpha$ can be correlated by a straight line and the activation energy can be calculated from the slope (Ozawa, 1970). Thus, a series of activation energy can be

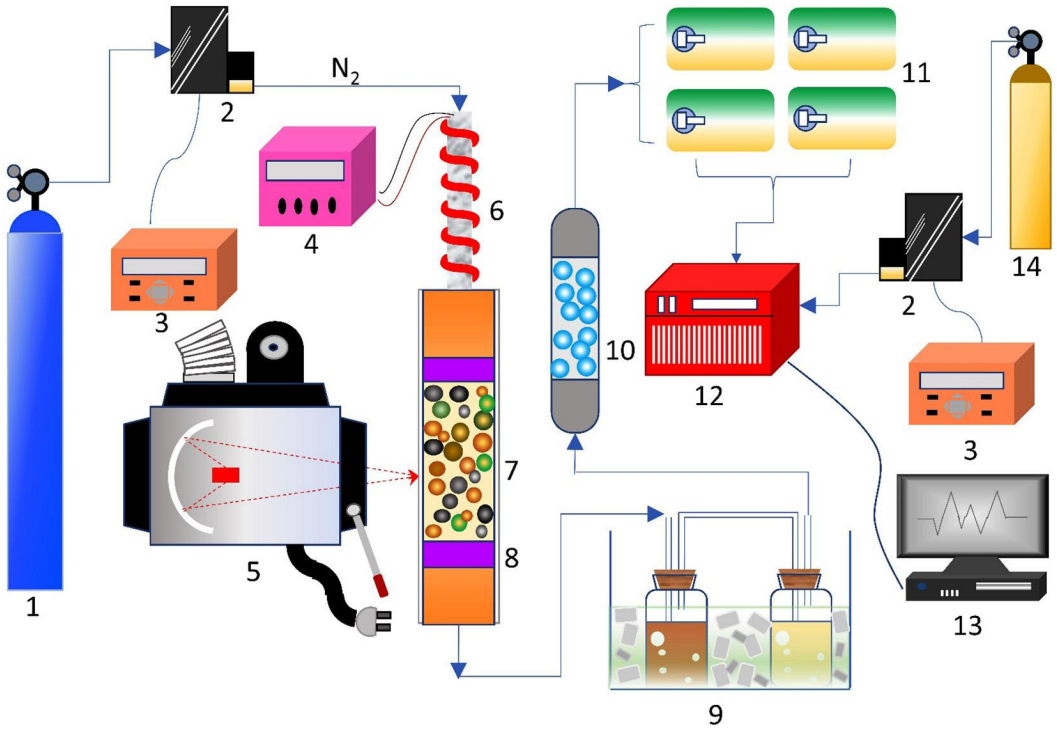

Fig. 1. Biomass pyrolysis setup using concentrated solar power. 1-nitrogen cylinder; 2-mass flow meter; 3-mass flow meter controller; 4-preheater controller; 5-solar simulator; 6-heating tape; 7-quartz glass reactor; 8-quartz wool/fritz; 9-bio-oil collector system; 10-moisture trap; 11-gas bags; 12-micro GC; 13-computer; 14- helium cylinder.

obtained corresponding to different α. The KAS method is also expressed seen as

$$\ln\left(\frac{\beta}{T_\alpha^2}\right) = \ln\left(\frac{AR}{g(\alpha)E_\alpha}\right) - \frac{E_\alpha}{RT_\alpha} \quad (15)$$

The activation energy is determined from the slope ($-E_\alpha/R$) of the straight line (Kissinger, 1957).

The parameter estimation using model-free methods do not depend on the mechanism of reactions. FWO and KAS methods are widely used for calculating activation energy and Arrhenius pre-exponential factor during pyrolysis of carbonaceous material. The activation energy is directly related to the fuel reactivity.

2.3. Solar pyrolysis of CS

About 2 g dry CS weighed and placed over the fritz inside the reactor. The reactor was swept with nitrogen from the top as shown in Fig. 1. The sample temperature was measured at a 1 s interval at the front and rear of the reactor. The solar flux was kept constant during the experiment and the reactor was placed at the focus of the solar simulator. The solar simulator can produce highly concentrated solar flux to heat the endothermic solar pyrolysis process (Rony et al., 2018). During the pyrolysis operation, liquid products including bio-oil and moisture were trapped in an ice-water cooling bath. After the experiment, the system was cooled, disassembled, and char was collected for weighing. To collect sticky bio-oil and tar from reactor wall and pipeline, acetone was used to wash the system. Gas was collected using gas-bags for further analysis during the pyrolysis operation. Each test was performed thrice, and mean value was taken.

2.4. Post pyrolysis characterization

2.4.1. Gel permeation chromatography (GPC)

The liquid collected during the solar pyrolysis process was dried using Na_2SO_4 desiccant was used to remove water and the desiccant was filtered out. The filter paper was then washed out using high purity acetone. The acetone was evaporated at room temperature using a centrifuge and pure tar was collected. Tetrahydrofuran (THF) was used as a solvent to dissolve the tar produced in this process. The mixture was filtered using 0.1 μm filter before being injected in the GPC column at a flow rate of 1.0 ml/min from the sample vial to an Agilent® 1260 infinity device. The columns used were PLgel 3um MIXED-E 200x7.5 mm from Agilent®. The signal was acquired by a Diode-array detector (DAD) detector of 270 nm, The GPC calibration was performed Polyethylene Glycol/Oxide (PEG / PEO) standards with molecular weight (MW) from 162 to 45120. The retention time limit was between 10.5 min and 20.5 min.

2.4.2. Gas chromatography

Mass spectroscopy (MS) enables detection of various compounds from the collected liquid. The liquid product first dried using a desiccant and filtered to remove any debris, bio-char, or grit. HPLC grade acetone was used as a solvent for bio-oil. An Agilent 5975C gas chromatograph/mass spectrometer (GC/MS) was used for the analysis. For product separation, an HP-5 MS Ultra Inert capillary column (30 m × 0.25 mm × 0.25 μm) was available. The GC column was kept at 40 °C for 180 s, then heated up to 300 °C at a heating rate of 3 K/min and the system kept at the isothermal condition for 600 s. To analyze the molecules from observed peaks, NIST/EPA/NIH Mass spectral library version 2.2 was used.

A Varian 400 Micro-GC was used to analyze the gas collected during the pyrolysis process. The gas was pushed into the micro-GC by an automatic pump and heated at 50 °C. The sampling time was 2 min with 5 s stabilization time.

3. Results and discussion

3.1. Material compositions

The proximate analysis shows that the fixed carbon, volatile,

moisture and ash of CS are 5.8%, 81.1%, 8.3%, and 4.8%, respectively. The CS was dried by the sunlight under atmospheric condition before collection to reduce moisture content at the source. The high volatile indicates that CS has tremendous potential as a source of bio-fuel because liquid chemicals originate from it. According to ultimate analysis results, the CS contains 46.5% C, 5.81% H, 0.56% N, 39.7% O, and 0.05% S on weight basis. The ICP-MS detects metal components as metal oxides from the ash content of CS. The ash analysis in terms of weight is as follows: SiO_2 = 31.94%, Al_2O_3 = 8.65%, Fe_2O_3 = 3.87%, MgO = 4.23%, CaO = 6.18%, TiO_2 = 0.35%, K_2O = 41.24%, Na_2O = 3.41%, MnO_2 = 0.10%, BaO = 0.04%. Ash content of CS is higher than woody biomass, thus a detail analysis was necessary because ash composition of biomass can have significant impact on overall biomass pyrolysis performance according to literature. According to literature, some of the components of biomass can have significant impact on overall biomass pyrolysis performance. CaO can enhance the hydrogen gas content during biomass pyrolysis by capturing CO_2 while also increase the char content as well (Han et al., 2010). Fe_2O_3-Al_2O_3 catalyst is known to have a positive impact on hydrogen production during biomass pyrolysis (Xu et al., 2012). Fe_2O_3 (hematite) can facilitate the breakdown of tar and oxidation of phenols produced during the pyrolysis process (Khelfa et al., 2009).

The higher heating value (HHV) of CS can be calculated by using

$$HHV(MJ/kg) = 0.338\ C + 1.428(H - O/8) + 0.095S \quad (16)$$

where C, H, O, and S are presence if carbon, hydrogen, oxygen and sulfur content in CS respectively on weight basis (Nhuchhen and Abdul Salam, 2012).

3.2. Thermal degradation process

The pyrolysis curve of CS obtained under nitrogen condition is shown in Fig. 2. CS, like other biomass material, has different components such as cellulose, hemicellulose, and lignin. The dry CS sample exhibits decomposition in two ways. One is active pyrolysis involving hemicellulose, cellulose, and a small fraction of lignin. The decomposition of cellulose involves CO, CO_2 generation and breakage of carbonaceous polymer bonds. At higher temperature these radicals associated to form liquid products. The other one, passive pyrolysis, mostly involves lignin components to produce mainly bio-char. As seen from Fig. 2, the active pyrolysis corresponds to the temperature range of 160 °C to 350 °C. The second zone, attributed to passive pyrolysis, ranges from 350 °C to 700 °C. As lignin can start decomposing as low as 200 °C, there is a possible overlap between the two regions as well. The long tailing of DTG curve can be associated to the slower decomposition of lignin. The positions of the two peaks are dependent on the heating rate of the pyrolysis process. The higher the heating rate, the higher are the two peak temperatures as observed from Fig. 2. At higher heating rate, the heat transfer efficiency is generally low because the core temperature would be relatively lower than the outer surface temperature. The heating rate also greatly affect the conversion process leading to different product distribution as well. The heating rate greatly affect the conversion process leading to different product distribution. Since solar intensity is kept constant during the solar pyrolysis experiment, the heating rate is variable due to heat transfer.

3.3. Kinetics models for CS pyrolysis

The TGA data was used to fit 14 different models to calculate the activation energy and R^2. Based on conversion (α), the datasets for each heating rate was divided into two regions ($0 \le \alpha \le 0.75$ and $0.75 < \alpha \le 1.0$) following the results obtained using FWO and KAS model. The types of the model chosen were: diffusion models, geometrical contraction models, reaction order models, power models, nucleation models. Among the kinetic models, zero order, 1-D diffusion, contracting area, contracting volume, Avrami-Erofeyev (A2) has R^2 value of more than 0.9 regardless of heating rate and conversion (α). Table 1 also list the range of R^2 value for each method. Following the results described in section 3.3, the entire datasets (for each heating rate) were divided into two region of conversion (α) and fitted separately. The relative error for each model was depicted in Fig. 5. None of the models can predict the activation energy for the entire region accurately but zero order method and Avrami-Erofeyev based model performs better. Both of the models are based on nucleation process. A bulk solid can have fluctuation of local energies due to surface, edges, cracks, impurities, and point defects to enable reaction nucleation on the site, nucleation site, at a lower activation energy. The pyrolysis might have followed the mechanism of lattice decomposition. The zero-order model can mean 1-D movement of phase boundary as a product nucleation mechanism. Interestingly, 1-D diffusion model also happens to be a better fit. Huang et al (Huang et al., 2016) has described the kinetics of a variety of biomass for microwave assisted pyrolysis using CR method to estimate rate constant, Activation energy, pre-exponential factor, rate constant, and time required for half the biomass sample reacted. Uzun and Sarioğlu (2009) has also described the pyrolysis behavior and kinetics for corn stover using CR method.

3.4. Model free kinetics

Fig. 3a and 3b show the FWO and KAS plots for of CS based pyrolysis processes. Both the FWO and the KAS methods for analysis of kinetics of biomass material during the pyrolysis process are becoming increasingly popular (Bach and Chen, 2017; White et al., 2011; Yuan et al., 2015). Sittisun et al. (2015) have studied the corn residue kinetics during the combustion process. They have calculated the activation energy of 170 kJ/mol and 148 kJ/mol respectively for FWO method

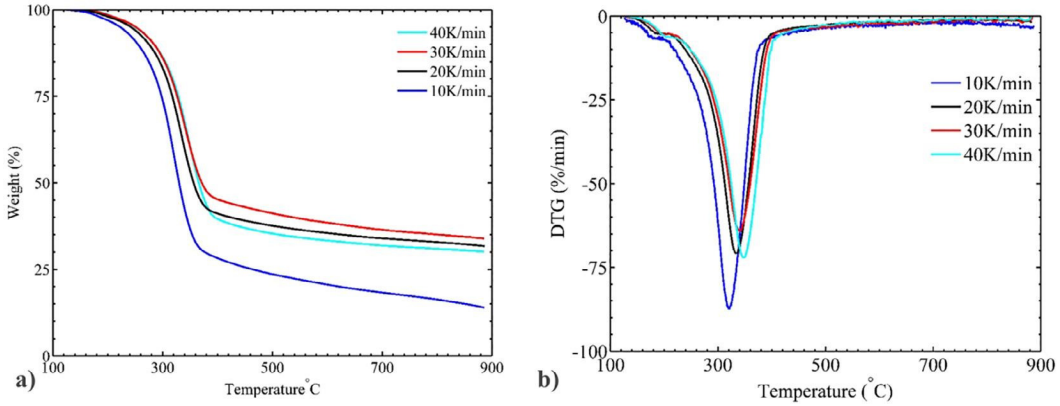

Fig. 2. TG and DTG curves of CS pyrolysis at different heating rates (10 K/min, 20 K/min, 30 K/min and 40 K/min). a) TG curves of CS; b) DTG curves of CS.

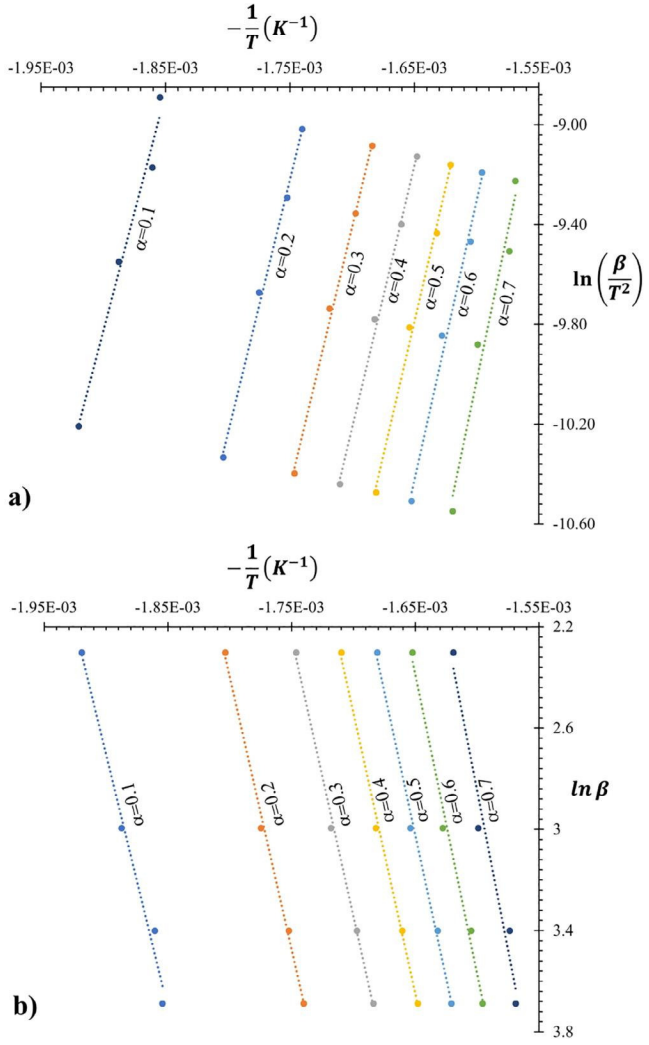

Fig. 3. Model-free kinetics. a) KAS model. B) FWO model.

and the KAS method. Slopiecka et al. (2012) have studied the kinetics of poplar wood using thermogravimetric analysis in nitrogen atmosphere. They reported the pyrolysis process as mainly active and passive along with dehydration process. The average activation energy of poplar wood was 158.58 kJ/mol and 157.27 kJ/mol respectively for FWO and KAS method. The devolatilization process was identified as first order according to the study. Islam et al. (2015) has studied Karanj fruit hulls as a pyrolysis feed material using TGA following FWO and KAS method. They have calculated the activation energy as 61.06 kJ/mol for KAS method and 135.87 kJ/mol for the FWO method for Karanj fruit hulls. The study found that lignin content was the key component to regulate the decomposition mechanism.

The mean activation energy (E_a) of CS calculated using KAS and FWO method was 181.66 kJ.mol^{-1} and 191.57 kJ.mol^{-1} respectively in this study. These values are consistent with literature value for traditional pyrolysis process (Islam et al., 2015; Sittisun et al., 2015; Slopiecka et al., 2012). The lower R^2 value (0.98–0.97) means that the models are good fit for the data. Since both KAS and FWO methods are based on first order reaction, the secondary reaction is not rate determining and has smaller impact on the overall reaction kinetics. The discrepancies (5%–6%) between the results from the two methods comes from the approximations to solve the temperature integral. However, KAS method is more reliable (error $<$ 2%) compared to FWO method according to literature (Farjas and Roura, 2011).

3.5. Thermodynamics of CS

Important thermodynamic parameters include Arrhenius pre-exponential factor (A), enthalpy (ΔH), Gibbs free energy(ΔG), and entropy (ΔS). ASTM E698 (Standard Test Method for Kinetic Parameters for Thermally Unstable Materials Using Differential Scanning Calorimetry and the Flynn/Wall/Ozawa Method, 2018) describes the method to determine Arrhenius pre-exponential factor along with activation energy. However, the method is limited to materials which exhibit behavior predicted by Arrhenius equation in which the Arrhenius pre-exponential factor (A) is given by the following equation

$$A = \frac{\beta E_\alpha exp\left(\frac{E_\alpha}{RT_m}\right)}{RT_m^2}$$

Enthalpy change (ΔH), Gibbs free energy (ΔG), and change of entropy (ΔS) are calculated in the way of

$$\Delta H = E_\alpha - RT \tag{18}$$

$$\Delta G = E_\alpha + RT_m ln\left(\frac{K_B T_m}{hA}\right) \tag{19}$$

$$\Delta S = \frac{\Delta H - \Delta G}{T_m} \tag{20}$$

Fig. 4 demonstrates the thermodynamic parameters of CS using FWO and KAS methods. The activation energy varies from 157.8 kJ/mole to 215.1 kJ/mol for KAS method, while for the FWO method the range of activation energy is 166.6–225.9 kJ/mol. It is generally defined as the energy needed to initiate a reaction. The Arrhenius exponential prefactor, implies the empirical relation between reaction rate coefficient and temperature, varies from 4.07*10^{12} s^{-1} to 7.08*10^{17} s^{-1} and 6.7*10^{11} s^{-1} to 7.97*10^{16} s^{-1} for FWO and KAS method respectively. The enthalpy, total heat content of the system, ranges from 162 to 221 kJ/mol for FWO method and 153–210 kJ/mol for KAS method. The Gibbs free energy may be inferred as the energy for the formation of activated complex. It is also the available energy from biomass associated with pyrolysis process The Gibbs free energy (171–172 kJ/mol) does not change much for either method for different conversion. The likelihood of the pyrolysis reaction can be determined from the difference between activation energy and enthalpy values. At thermodynamic equilibrium, change in Gibbs free energy is 0. Since the products are withdrawn from the system continuously, the system never reaches true thermodynamic equilibria as evidenced from the results. The Entropy, the measure of disorder, changes from −16 J/K to 82 J/K for FWO method and for KAS method Entropy changes from −31 J/K to 63.5 J/K. As biomass pyrolysis is a complex process, negative entropy value can occur. It is possible to have a lower degree of disorder of the products compared to the reactants due to the bond dissociation. A lower value of ΔS may relates to only physical change and little chemical reactivity. However, higher reactivity and rapid activated complex formation is marked by higher value of ΔS. Kaur et al (Kaur et al., 2018) described the thermodynamics of castor residue pyrolysis for room temperature to 900 °C using TGA to analyze bioenergy production potential. They calculated the Gibbs free energy 150.59–154.65 kJ/mol for castor residue. Chen et al (Chen et al., 2017) calculated the Gibbs free energy 182.89 kJ/mol for rape straw and 172.39 kJ/mol for wheat bran. Ahmad et al (Ahmad et al., 2018) determined the Gibbs free energy for *Wolffia arrhizal* (an aquatic plant) as 171 kJ/mol.

3.6. Biomass pyrolysis products

Bio-oil was collected from solar pyrolysis system and analyzed in GC–MS. The gas components were analyzed using micro-GC. The gas stream consisted of CO_2, CH_4, H_2, CO and other lighter hydrocarbons (C_2-C_4). The pyrolysis process essentially breaks the structure of

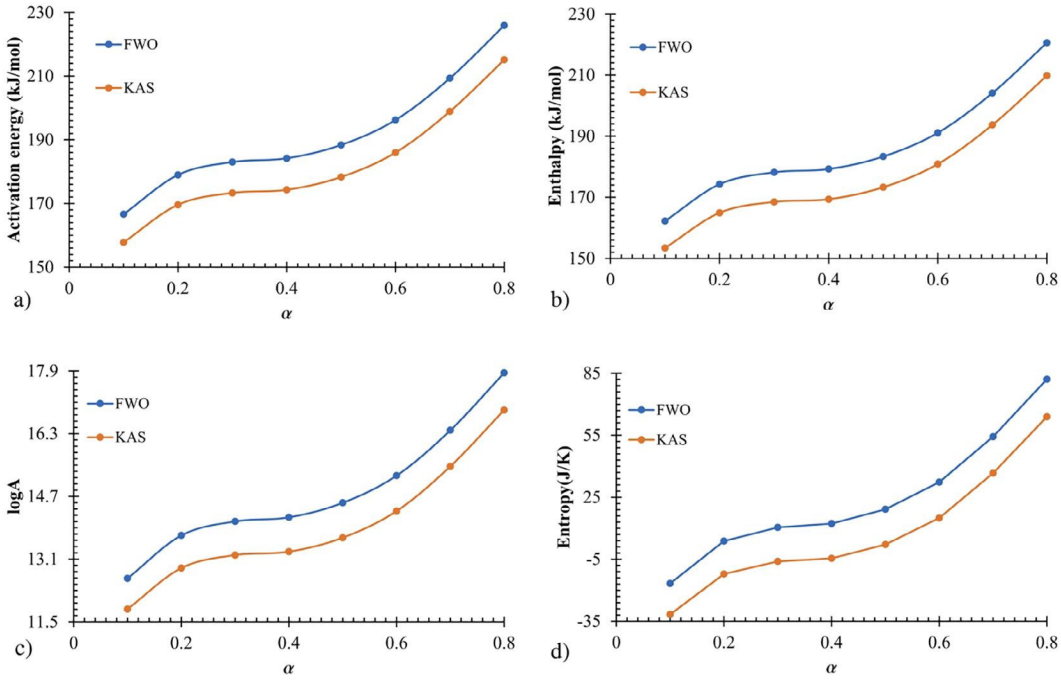

Fig. 4. Change in thermodynamics and kinetics parameters of CS using FWO and KAS method at different conversion. a) Activation energy vs conversion b) Enthalpy vs conversion c) $\log_{10}$(Arrhenius pre-exponential factor) vs conversion, d) Entropy vs conversion.

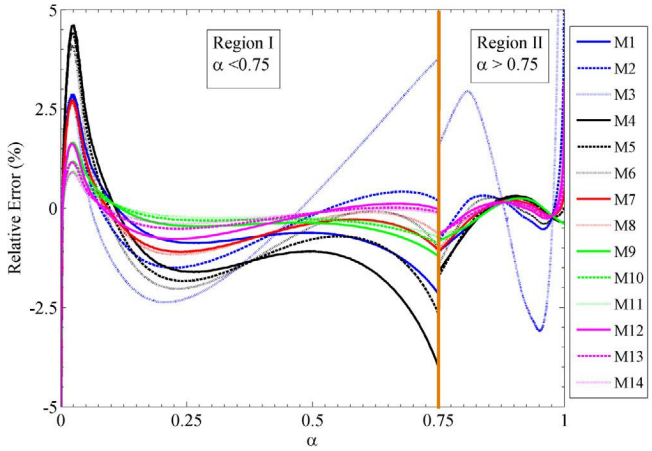

Fig. 5. Relative error (%) for different kinetic models of CS depends on the conversion (α). [M1-Zero order, M2-1st order, M3-2nd order, M4-1D diffusion, M5-2D diffusion M6-3-D diffusion-Jander, M7-Contracting area, M8-Contracting volume, M9-power model (P2) M10-power model (P3), M11-power model (P4), M12-Avrami-Erofeyev (A2), M12-Avrami-Erofeyev (A3), M12-Avrami-Erofeyev (A4)].

biomass and strip off various material which leads to both gaseous and liquid product. The liquid product consists of numerous compounds, but they can be categorized into different groups. The liquid is consisted of 44% phenols, 13% furans, 5% ketones, 5% aromatics, 3% amines, and others 30%. The 'others group' consisted of undetectable compounds, aldehydes, acids, linear alkanes, alkynes, *cyclo*-alkane etc.

3.7. Molar-mass dispersity

GPC technology allows characterization of molecules in terms of size. MW (molecular weight) and distribution of products can be analyzed using this technic. Molar-mass dispersity (also known as 'Polydispersity index') can be defined as, $D_M = M_w/M_n$. For a bio-oil mixture, the weight average molecular weight (Mw) means the molecular weight of the average molecules present. The number average molecular weight (Mn) is defined as the number of average molecules in the mixture. The results show that bio-oil produced from CS using concentrated solar light has molar-mass dispersity of 1.02. For $D_M = 1$, it can be inferred that the polymer is perfectly uniform. It is evident that the bio-oil is a homogeneous mixture of polymers.

4. Conclusions

The studied CS contains 81.1% volatile compounds and its heating value is 16.22 MJ/kg. The average activation energies of CS pyrolysis with FWO and KAS models are 191.57 kJ/mole and 181.66 kJ/mol, respectively. Among tested other kinetics models, 1-D diffusion one well fits the kinetic data with its R^2 value being higher than 0.94. The corresponding Gibbs free energies of the pyrolysis process are about 172 kJ/mole. The oil produced from the CS contains as high as 44% phenols and 13% furans. The results indicate that the CS can be a great bioresource for chemical production with solar pyrolysis.

Acknowledgement

The authors thank the National Science Foundation (NSF OIA-1632899) for their support to this research.

Conflict of interest

The authors declare no conflict of interest.

Appendix A. Supplementary data

Supplementary data to this article can be found online at https://doi.org/10.1016/j.biortech.2019.03.049.

References

Ahmad, M.S., Mehmood, M.A., Liu, C.-G., Tawab, A., Bai, F.-W., Sakdaronnarong, C., Xu, J., Rahimuddin, S.A., Gull, M., 2018. Bioenergy potential of Wolffia arrhiza appraised through pyrolysis, kinetics, thermodynamics parameters and TG-FTIR-MS study of

the evolved gases. Bioresour. Technol.
Angel Gurría, 2012. OECD Green Growth Studies, oecd.org. doi:10.1787/9789264115118-en.
Anwar, Z., Gulfraz, M., Irshad, M., 2014. Agro-industrial lignocellulosic biomass a key to unlock the future bio-energy: a brief review. J. Radiat. Res. Appl. Sci. 7, 163–173. https://doi.org/10.1016/j.jrras.2014.02.003.
ASTM D3172-13 ASTM International, 2013. D3172-13 Standard Practice for Proximate Analysis of Coal and Coke. doi:10.1520/D3172-13.
ASTM E698 Standard Test Method for Kinetic Parameters for Thermally Unstable Materials Using Differential Scanning Calorimetry and the Flynn/Wall/Ozawa Method, 2018. West Conshohocken, PA. doi:10.1520/E0698-18.
Bach, Q.-V., Chen, W.-H., 2017. A comprehensive study on pyrolysis kinetics of microalgal biomass. Energy Convers. Manage. 131, 109–116. https://doi.org/10.1016/J.ENCONMAN.2016.10.077.
Biney, P.O., Gyamerah, M., Shen, J., Menezes, B., 2015. Kinetics of the pyrolysis of arundo, sawdust, corn stover and switch grass biomass by thermogravimetric analysis using a multi-stage model. Bioresour. Technol. 179, 113–122. https://doi.org/10.1016/J.BIORTECH.2014.10.155.
Bridgwater, A.V., 2012. Review of fast pyrolysis of biomass and product upgrading. Biomass Bioenergy 38, 68–94. https://doi.org/10.1016/j.biombioe.2011.01.048.
Bridgwater, A., 2003. Renewable fuels and chemicals by thermal processing of biomass. Chem. Eng. J. 91, 87–102. https://doi.org/10.1016/S1385-8947(02)00142-0.
Cai, J., Xu, D., Dong, Z., Yu, X., Yang, Y., Banks, S.W., Bridgwater, A.V., 2018. Processing thermogravimetric analysis data for isoconversional kinetic analysis of lignocellulosic biomass pyrolysis: case study of corn stalk. Renew. Sustain. Energy Rev. 82, 2705–2715. https://doi.org/10.1016/J.RSER.2017.09.113.
Chen, J., Wang, Y., Lang, X., Ren, X., Fan, S., et al., 2017. Evaluation of agricultural residues pyrolysis under non-isothermal conditions: thermal behaviors, kinetics, and thermodynamics. Bioresour. Technol. 241.
Chen, W.H., Lu, K.M., Lee, W.J., Liu, S.H., Lin, T.C., 2014. Non-oxidative and oxidative torrefaction characterization and SEM observations of fibrous and ligneous biomass. Appl. Energy 114, 104–113. https://doi.org/10.1016/j.apenergy.2013.09.045.
Chintala, V., 2018. Production, upgradation and utilization of solar assisted pyrolysis fuels from biomass – A technical review. Renew. Sustain. Energy Rev. 90, 120–130. https://doi.org/10.1016/J.RSER.2018.03.066.
Chintala, V., Kumar, S., Pandey, J.K., Sharma, A.K., Kumar, S., 2017. Solar thermal pyrolysis of non-edible seeds to biofuels and their feasibility assessment. Energy Convers. Manage. 153, 482–492. https://doi.org/10.1016/J.ENCONMAN.2017.10.029.
COATS, REDFERN, 1964. Kinetic parameters from thermogravimetric data. Nature 201, 68–69. https://doi.org/10.1038/201068a0.
Fantini, M., 2017. Biomass availability, potential and characteristics, in: Lecture Notes in Energy. pp. 21–54. doi:10.1007/978-3-319-48288-0_2.
Farjas, J., Roura, P., 2011. Isoconversional analysis of solid state transformations. J. Therm. Anal. Calorim. 105, 757–766. https://doi.org/10.1007/s10973-011-1446-4.
Foley, A., Olabi, A.G., 2017. Renewable energy technology developments, trends and policy implications that can underpin the drive for global climate change. Renew. Sustain. Energy Rev. 68, 1112–1114. https://doi.org/10.1016/j.rser.2016.12.065.
Han, L., Wang, Q., Ma, Q., Yu, C., Luo, Z., Cen, K., 2010. Influence of CaO additives on wheat-straw pyrolysis as determined by TG-FTIR analysis. J. Anal. Appl. Pyrolysis 88, 199–206. https://doi.org/10.1016/J.JAAP.2010.04.007.
Huang, Y.-F., Chiueh, P.-T., Kuan, W.-H., Lo, S.-L., 2016. Microwave pyrolysis of lignocellulosic biomass: heating performance and reaction kinetics. Energy 100, 137–144. https://doi.org/10.1016/J.ENERGY.2016.01.088.
Islam, M.A., Asif, M., Hameed, B.H., 2015. Pyrolysis kinetics of raw and hydrothermally carbonized Karanj (Pongamia pinnata) fruit hulls via thermogravimetric analysis. Bioresour. Technol. 179, 227–233.
Kaur, R., Gera, P., Jha, M.K., Bhaskar, T., 2018. Pyrolysis kinetics and thermodynamic parameters of castor (Ricinus communis) residue using thermogravimetric analysis. Bioresour. Technol. 250, 422–428.
Khelfa, A., Sharypov, V., Finqueneisel, G., Weber, J.V., 2009. Catalytic pyrolysis and gasification of Miscanthus Giganteus: Haematite (Fe_2O_3) a versatile catalyst. J. Anal. Appl. Pyrolysis 84, 84–88. https://doi.org/10.1016/J.JAAP.2008.11.009.
Kim, S., Dale, B.E., 2016. A distributed cellulosic biorefinery system in the US Midwest based on corn stover. Biofuels Bioprod. Biorefin. 10, 819–832. https://doi.org/10.1002/bbb.1712.
Kim, S., Holtzapple, M.T., 2005. Lime pretreatment and enzymatic hydrolysis of corn stover. Bioresour. Technol. 96, 1994–2006. https://doi.org/10.1016/j.biortech.2005.01.014.
Kim, T.H., Kim, J.S., Sunwoo, C., Lee, Y.Y., 2003. Pretreatment of corn stover by aqueous ammonia. Bioresour. Technol. 90, 39–47. https://doi.org/10.1016/S0960-8524(03)00097-X.
Kim, S., Zhang, X., Dale, B., Reddy, A.D., Jones, C.D., Cronin, K., Izaurralde, R.C., Runge, T., Sharara, M., et al., 2018. Corn stover cannot simultaneously meet both the volume and GHG reduction requirements of the renewable fuel standard,. Wiley-Blackwell. Biofuels Bioprod. Biorefin. https://doi.org/10.1002/bbb.1830.
Kissinger, H.E., 1957. Reaction kinetics in differential thermal analysis. Anal. Chem. 29, 1702–1706. https://doi.org/10.1021/ac60131a045.
Meier, A., Steinfeld, A., 2010. Solar thermochemical production of fuels. Adv. Sci. Technol. 74, 303–312. https://doi.org/10.4028/www.scientific.net/AST.74.303.
Mishra, R.K., Mohanty, K., 2018. Pyrolysis kinetics and thermal behavior of waste sawdust biomass using thermogravimetric analysis. Bioresour. Technol. 251, 63–74. https://doi.org/10.1016/J.BIORTECH.2017.12.029.
Nhuchhen, D.R., Abdul Salam, P., 2012. Estimation of higher heating value of biomass from proximate analysis: a new approach. Fuel 99, 55–63. https://doi.org/10.1016/J.FUEL.2012.04.015.
Ozawa, T., 1970. Kinetic analysis of derivative curves in thermal analysis. J. Therm. Anal. 2, 301–324. https://doi.org/10.1007/BF01911411.
Perlack, R.D., Stokes, B.J., 2011. US billion-ton update. Biomass supply for a bioenergy and bioproducts industry. Renew. Energy 7, 1–227. https://doi.org/10.1089/ind.2011.7.375.
Pordesimo, L.O., Hames, B.R., Sokhansanj, S., Edens, W.C., 2005. Variation in corn stover composition and energy content with crop maturity. Biomass Bioenergy 28, 366–374. https://doi.org/10.1016/j.biombioe.2004.09.003.
Rafiq, M.K., Bachmann, R.T., Rafiq, M.T., Shang, Z., Joseph, S., Long, R., 2016. Influence of pyrolysis temperature on physico-chemical properties of corn stover (Zea mays L.) biochar and feasibility for carbon capture and energy balance. PLoS One 11, e0156894. https://doi.org/10.1371/journal.pone.0156894.
Rony, A.H., Mosiman, D., Sun, Z., Qin, D., Zheng, Y., Boman, J.H., Fan, M., 2018. A novel solar powered biomass pyrolysis reactor for producing fuels and chemicals. J. Anal. Appl. Pyrolysis 132, 19–32. https://doi.org/10.1016/J.JAAP.2018.03.020.
Sánchez, M., Clifford, B., Nixon, J.D., 2018. Modelling and evaluating a solar pyrolysis system. Renew. Energy 116, 630–638. https://doi.org/10.1016/J.RENENE.2017.10.023.
Sheehan, J., Aden, A., Paustian, K., Killian, K., Brenner, J., Walsh, M., Nelson, R., 2003. Energy and environmental aspects of using corn stover for fuel ethanol. J. Ind. Ecol. 7, 117–146. https://doi.org/10.1162/108819803323059433.
Sittisun, P., Tippayawong, N., Wattanasiriwech, D., 2015. Thermal degradation characteristics and kinetics of oxy combustion of corn residues. Adv. Mater. Sci. Eng. 2015, 1–8. https://doi.org/10.1155/2015/304395.
Slopiecka, K., Bartocci, P., Fantozzi, F., 2012. Thermogravimetric analysis and kinetic study of poplar wood pyrolysis. Appl. Energy 97, 491–497. https://doi.org/10.1016/J.APENERGY.2011.12.056.
Tao, L., He, X., Tan, E.C.D., Zhang, M., Aden, A., 2014. Comparative techno-economic analysis and reviews of n-butanol production from corn grain and corn stover. Biofuels, Bioprod. Biorefining 8, 342–361. https://doi.org/10.1002/bbb.1462.
Templeton, D.W., Sluiter, A.D., Hayward, T.K., Hames, B.R., Thomas, S.R., 2009. Assessing corn stover composition and sources of variability via NIRS. Cellulose 16, 621–639. https://doi.org/10.1007/s10570-009-9325-x.
UNFCCC, 2015. Clean development mechanism: CDM methodology booklet. United Nations Framework Convention on Climate Change, Bonn.
Uzun, B.B., Sarioğlu, N., 2009. Rapid and catalytic pyrolysis of corn stalks. Fuel Process. Technol. 90, 705–716. https://doi.org/10.1016/J.FUPROC.2009.01.012.
Wang, S., Dai, G., Yang, H., Luo, Z., 2017. Lignocellulosic biomass pyrolysis mechanism: a state-of-the-art review. Prog. Energy Combust. Sci. 62, 33–86. https://doi.org/10.1016/J.PECS.2017.05.004.
Weldekidan, H., Strezov, V., Town, G., Kan, T., 2018. Production and analysis of fuels and chemicals obtained from rice husk pyrolysis with concentrated solar radiation. Fuel 233, 396–403. https://doi.org/10.1016/J.FUEL.2018.06.061.
White, J.E., Catallo, W.J., Legendre, B.L., 2011. Biomass pyrolysis kinetics: a comparative critical review with relevant agricultural residue case studies. J. Anal. Appl. Pyrolysis 91, 1–33. https://doi.org/10.1016/J.J.
Xu, X., Enchen, J., Mingfeng, W., Bosong, L., Ling, Z., 2012. Hydrogen production by catalytic cracking of rice husk over Fe_2O_3/γ-Al_2O_3 catalyst. Renew. Energy 41, 23–28. https://doi.org/10.1016/j.renene.2011.09.004.
Yadav, D., Banerjee, R., 2016. A review of solar thermochemical processes. Renew. Sustain. Energy Rev. 54, 497–532. https://doi.org/10.1016/J.RSER.2015.10.026.
Yuan, T., Tahmasebi, A., Yu, J., 2015. Comparative study on pyrolysis of lignocellulosic and algal biomass using a thermogravimetric and a fixed-bed reactor. Bioresour. Technol. 175, 333–341. https://doi.org/10.1016/J.B.
Zeng, K., Gauthier, D., Soria, J., Mazza, G., Flamant, G., 2017. Solar pyrolysis of carbonaceous feedstocks: a review. Sol. Energy 156, 73–92. https://doi.org/10.1016/J.SOLENER.2017.05.033.